Supplementary Materials for

Extreme Dry and Humid Heat Seasons Are Changing Asymmetrically

Catherine C. Ivanovich[1,2*], Benjamin I. Cook[1,3], and Sonali McDermid[1,4]

[1] NASA Goddard Institute for Space Studies, New York, New York
[2] NASA Postdoctoral Program Fellow, Oak Ridge Associated Universities, NASA NPP Program, Oak Ridge, TN
[3] Division of Ocean Climate Physics, Lamont-Doherty Earth Observatory, Palisades, New York
[4] Department of Environmental Studies, New York University, New York, New York

**Correspondence to:* Catherine Ivanovich (cci2107@columbia.edu)

Contents of this file:

Figures S1 to S20

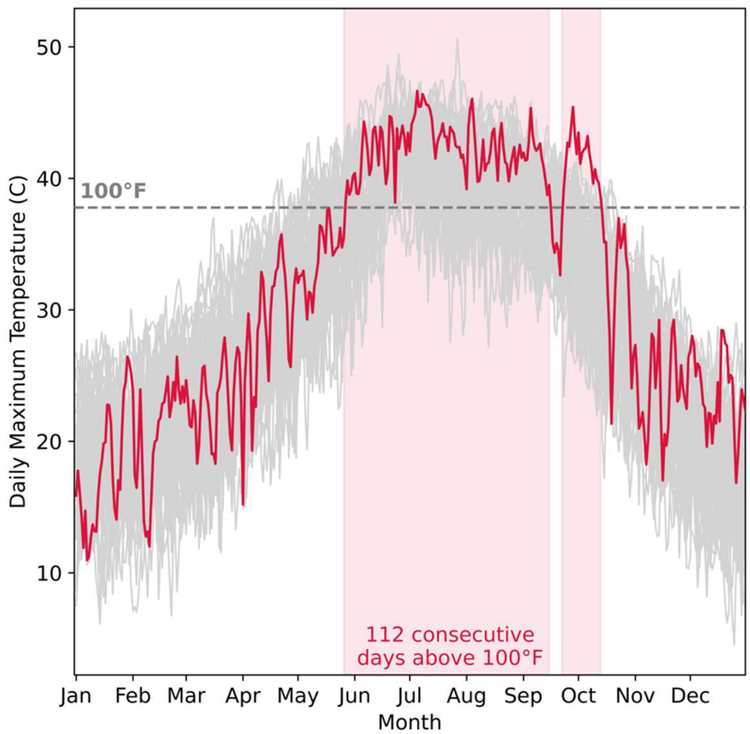

Figure S1: Phoenix's extreme heat season of 2024. Daily maximum temperature data from the grid cell closest to Phoenix, AZ in MERRA2. Time series for 2024 shown in red; time series for years 1980-2023 in grey. Consecutive days above 100°F shaded in red. The number of consecutive days above 100°F reported by MERRA2 is slightly different from those recorded by local weather stations.

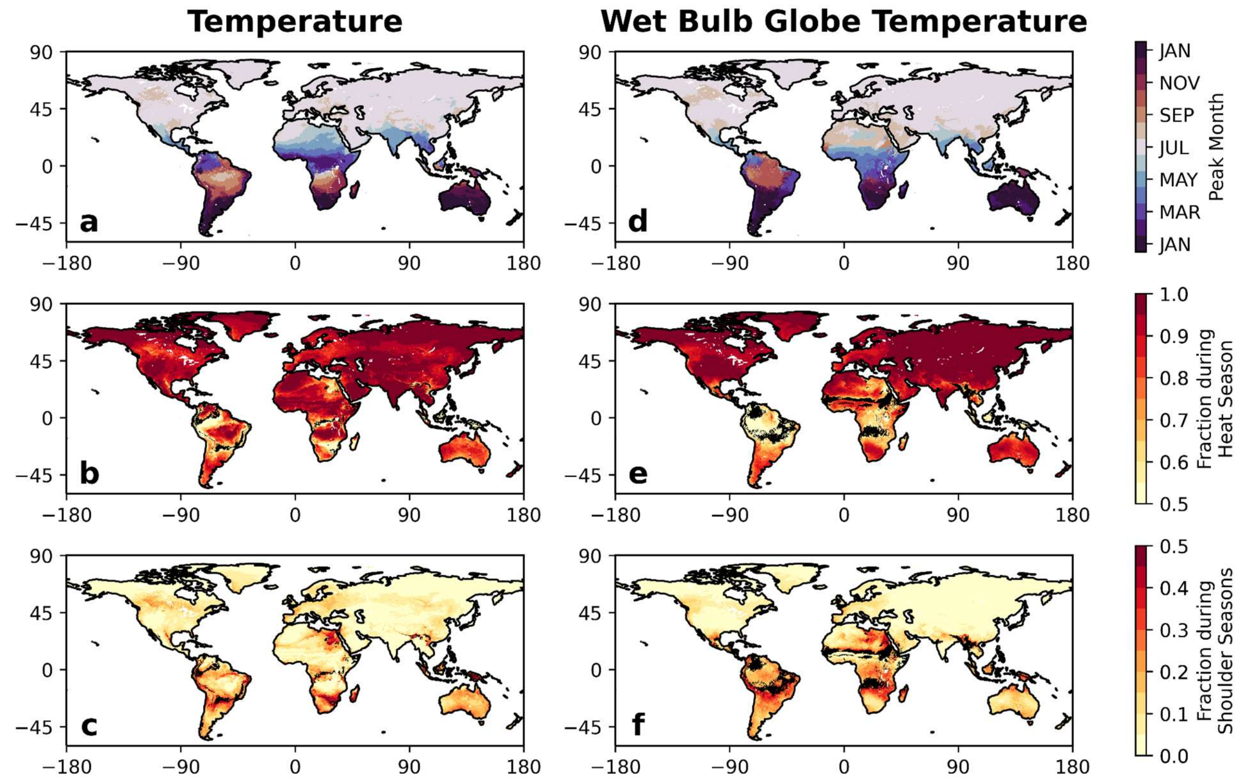

Figure S2: Analogous to Figure 2, reproduced using ERA5 data.

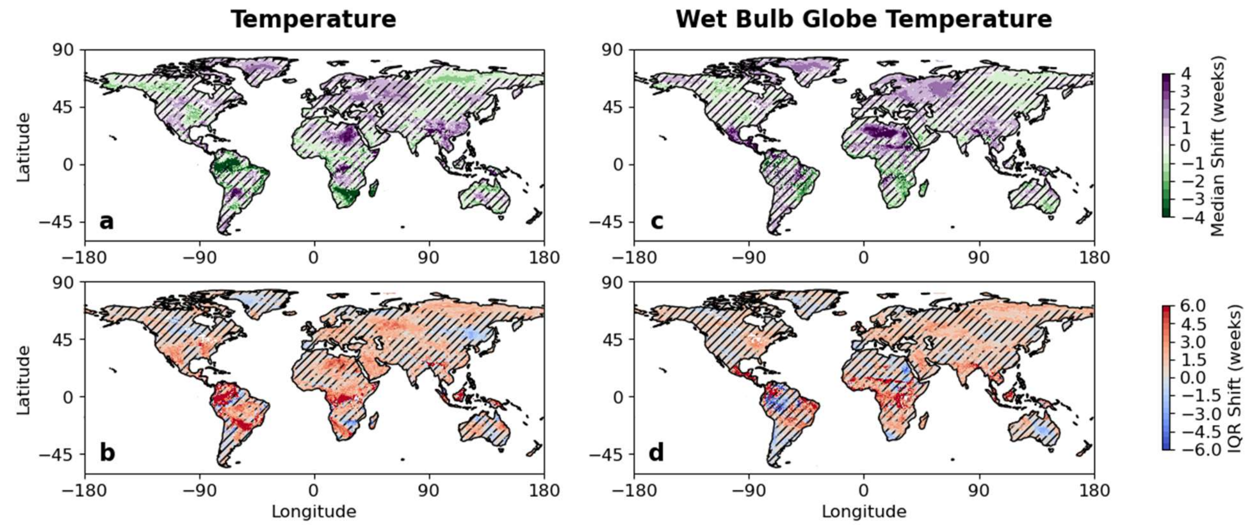

Figure S3: Analogous to Figure 3, reproduced using ERA5 data.

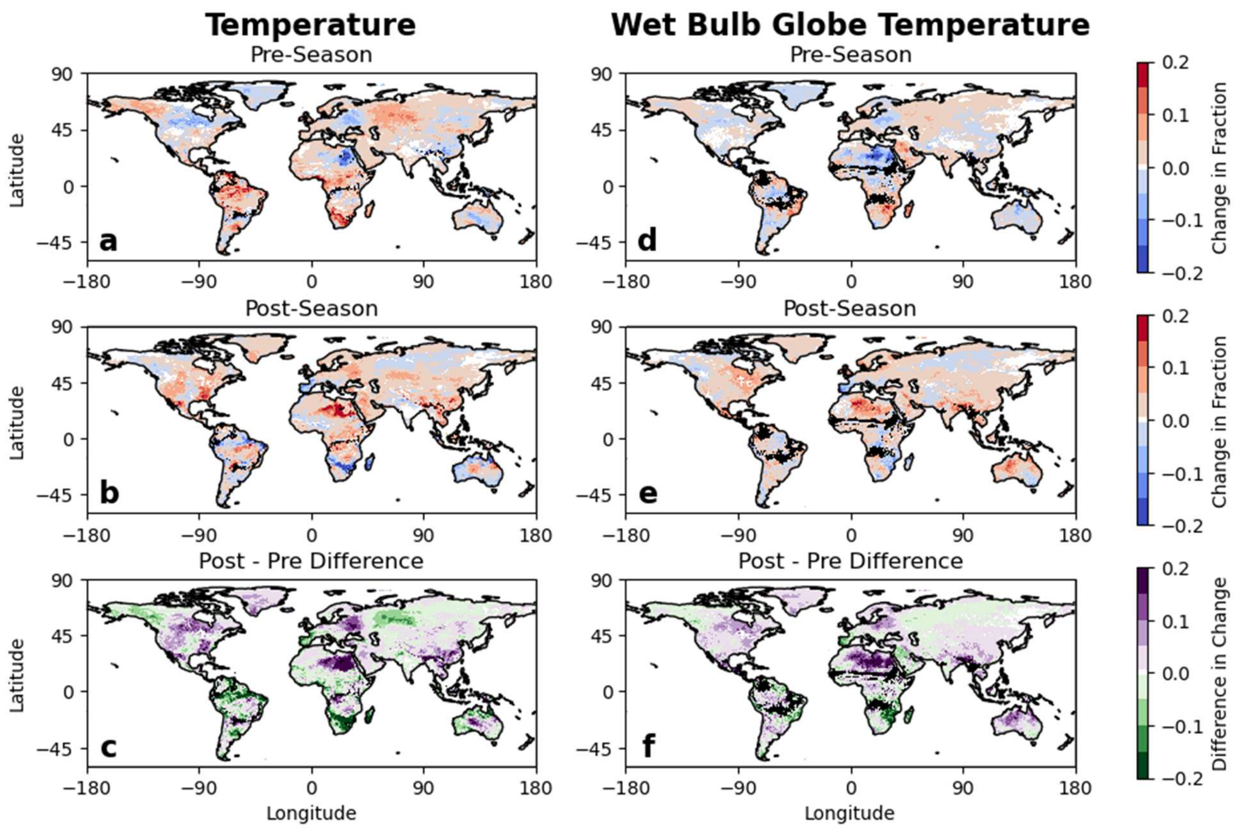

Figure S4: Analogous to Figure 4, reproduced using ERA5 data.

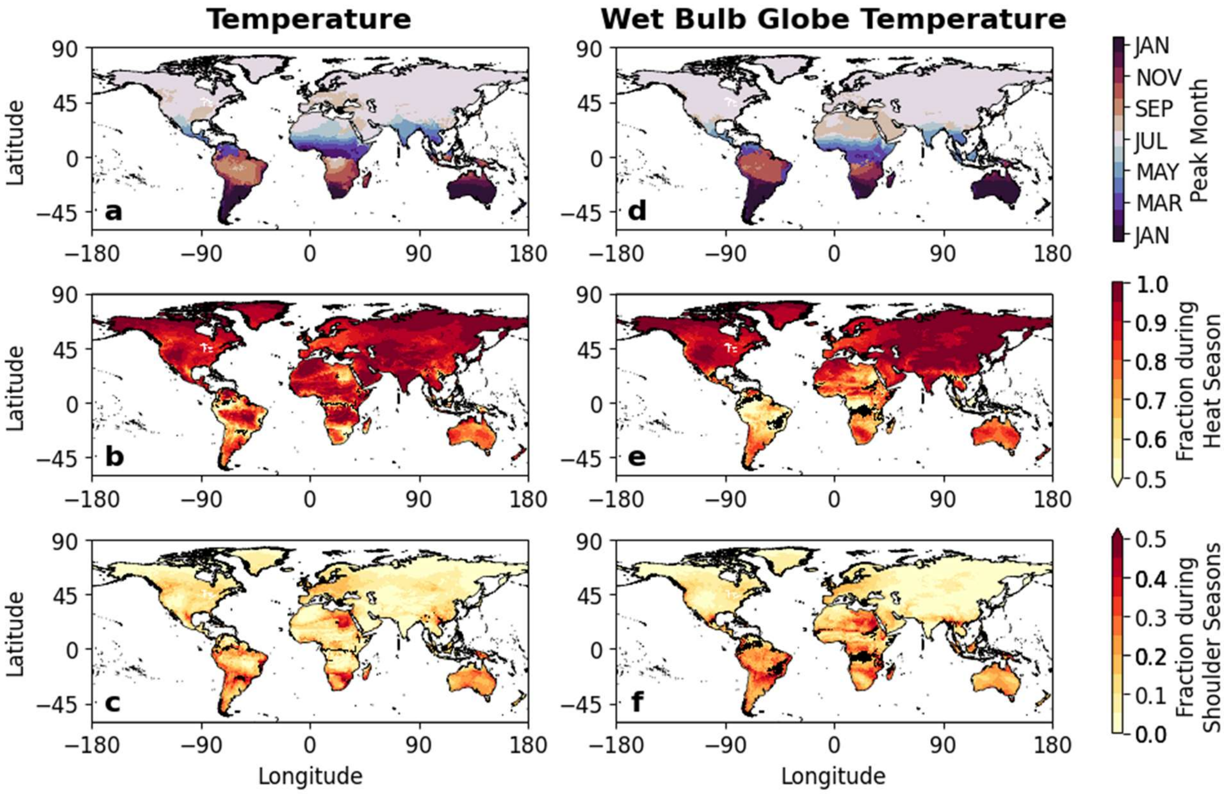

Figure S5: Figure 2 reproduced using 90th percentiles in temperature and WBGT as extreme thresholds (calculated from baseline period 1980-1989).

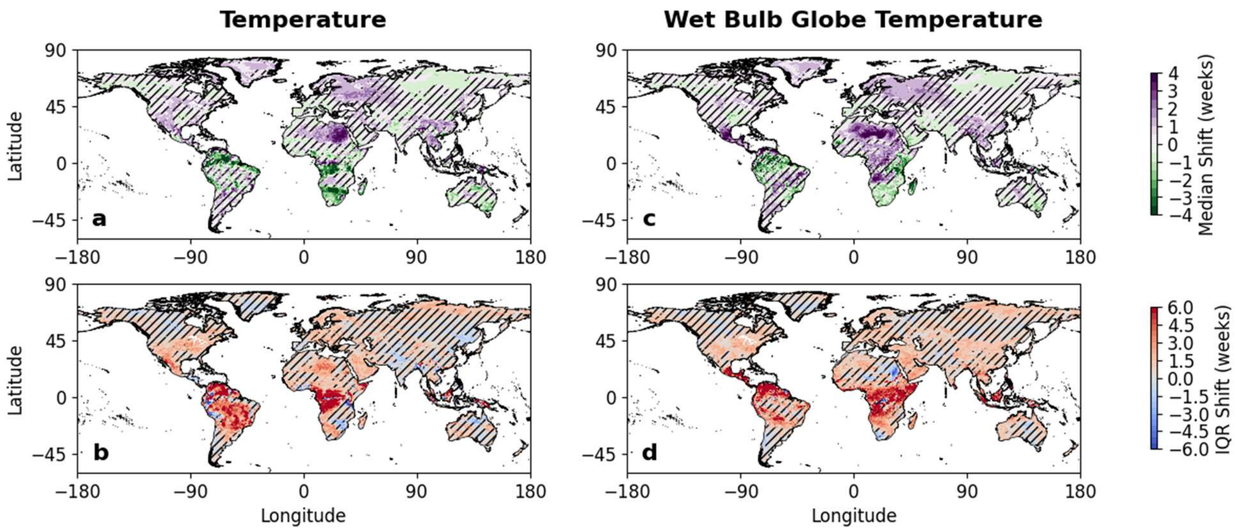

Figure S6: Figure 3 reproduced using 90th percentiles in temperature and WBGT as extreme thresholds (calculated from baseline period 1980-1989).

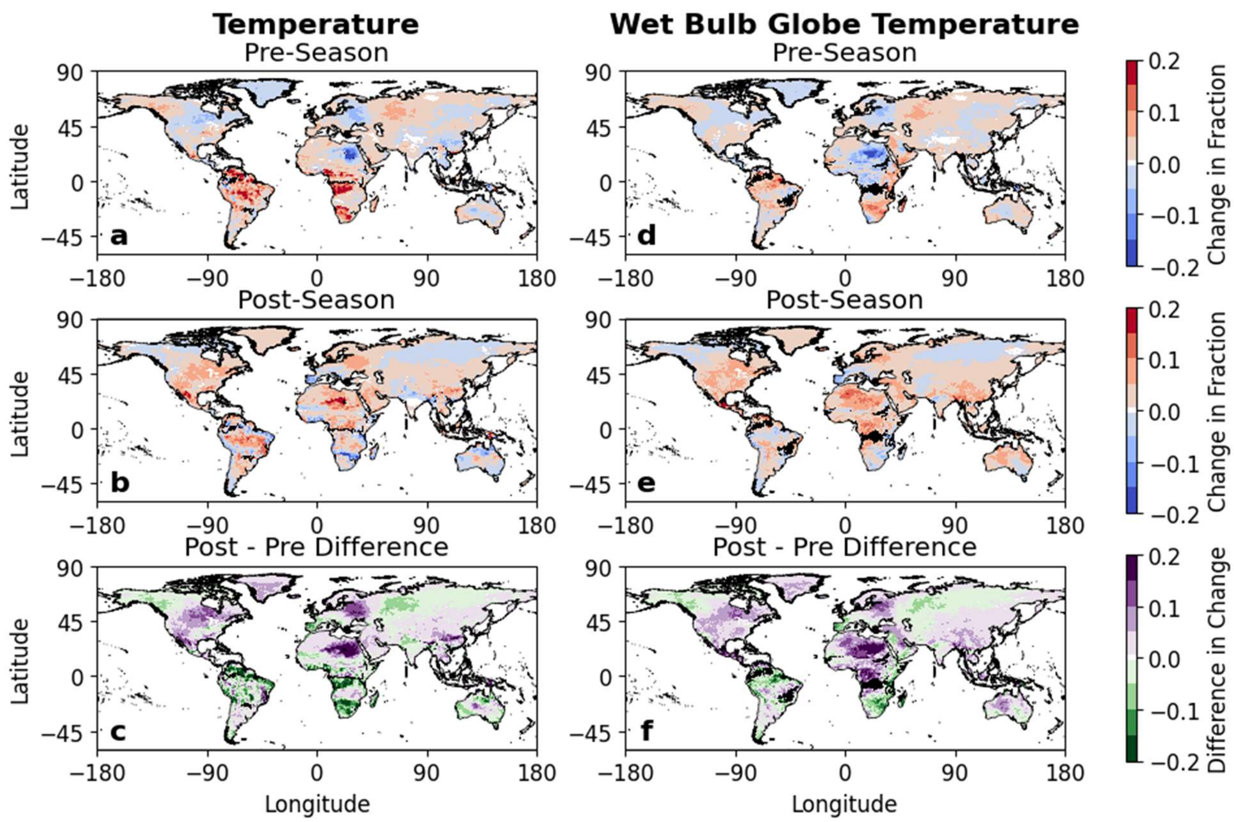

Figure S7: Figure 4 reproduced using 90th percentiles in temperature and WBGT as extreme thresholds (calculated from baseline period 1980-1989).

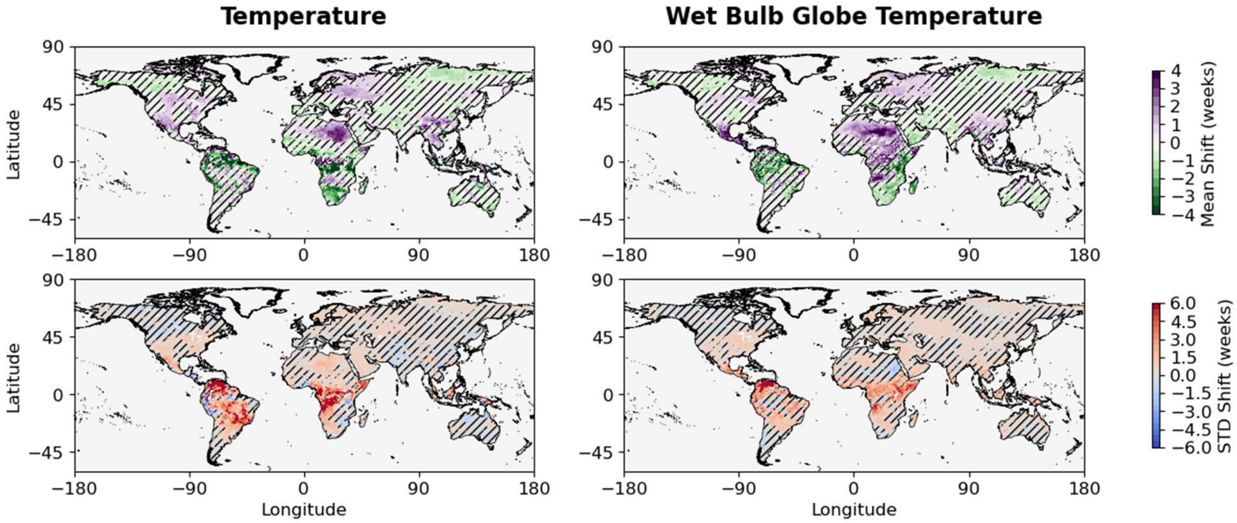

Figure S8: Analogous to Figure 3, but for changes in mean (top) and standard deviation (bottom).

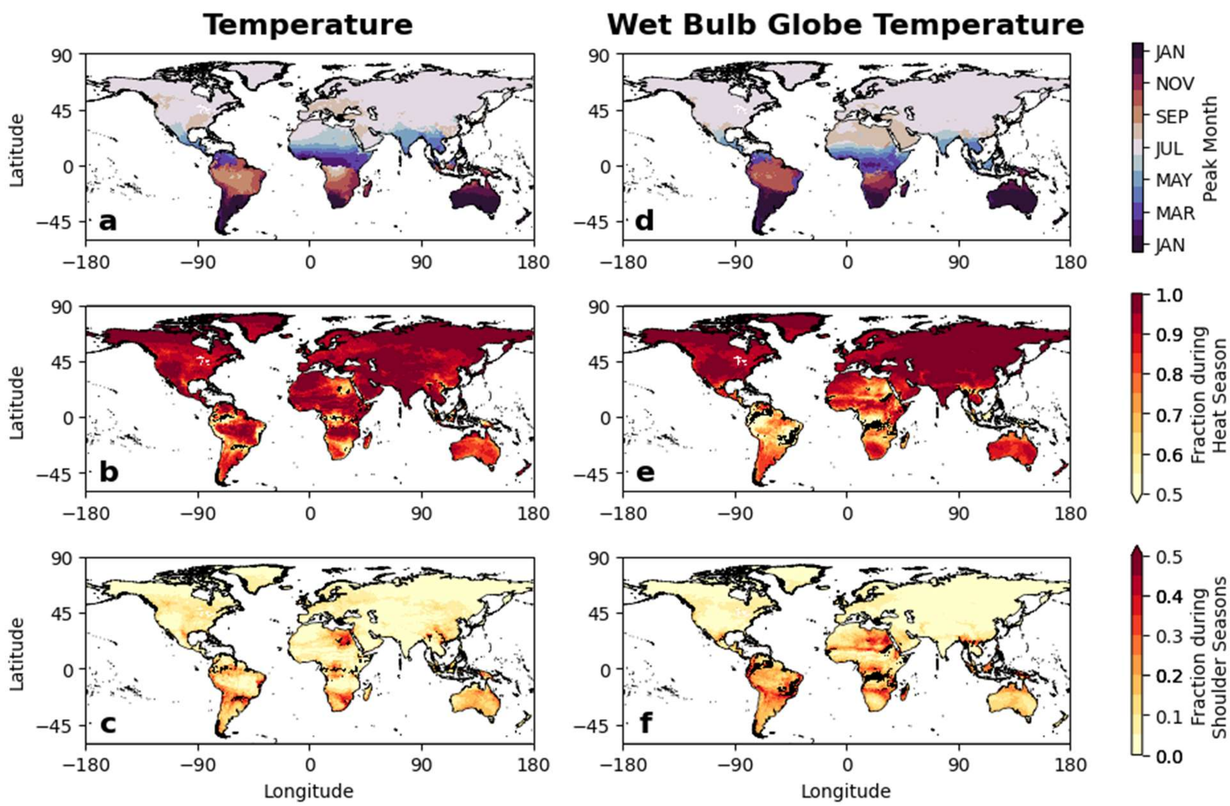

Figure S9: Reproduction of Figure 2, using a 15-year baseline period from 1980-1994.

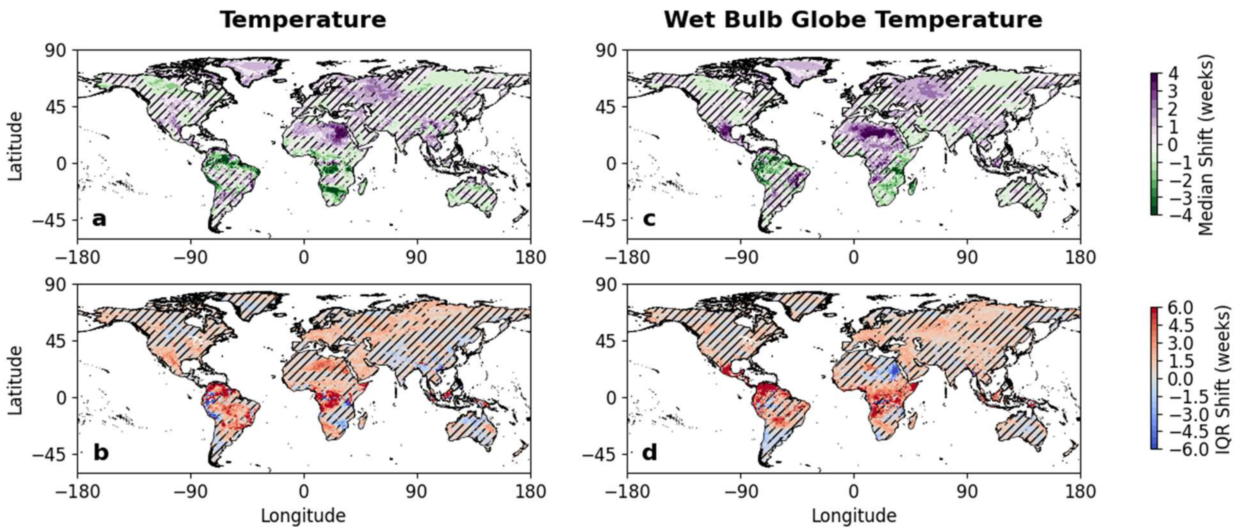

Figure S10: Reproduction of Figure 3, using a 15 year-baseline period from 1980-1994 and a 15-year recent historical period from 2010-2024.

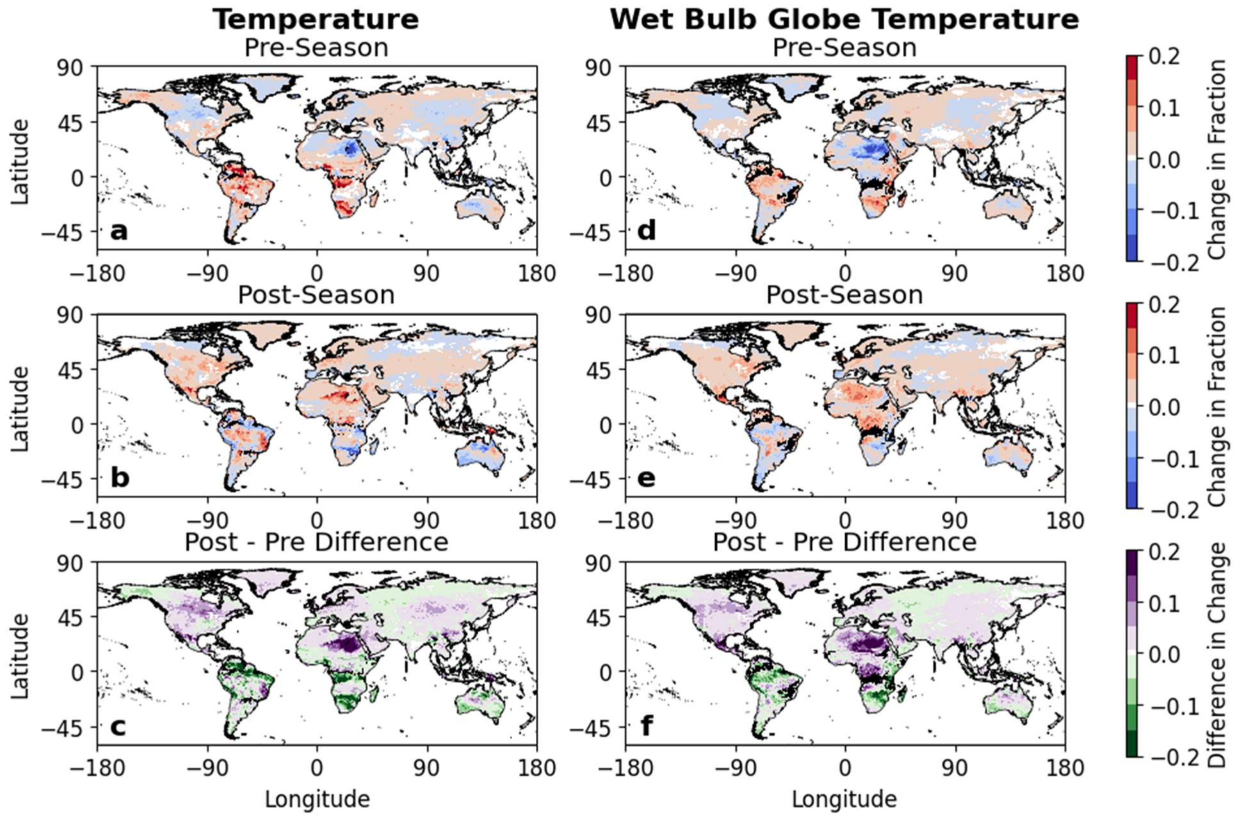

Figure 11: Reproduction of Figure 4, using a 15 year-baseline period from 1980-1994 and a 15-year recent historical period from 2010-2024.

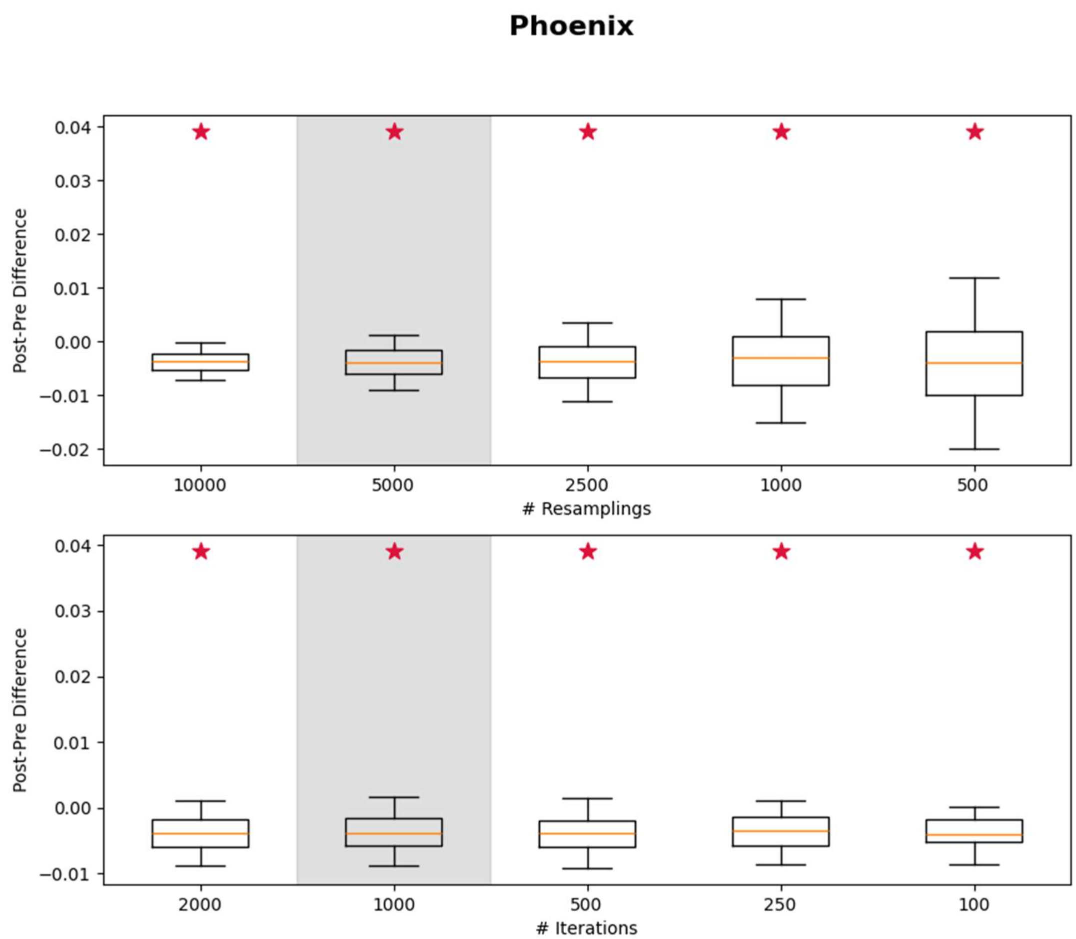

Figure S12: Bootstrapping sensitivity test for grid cell in Phoenix, Arizona. Box plots show the median, interquartile range, and 5th and 95th percentiles in the difference in the synthetic time series' post- versus pre-season fractional share of annual T95 events, as measured by bootstrapping tests with different numbers of resamplings and iterations. Star shows observed post- versus pre-season share of T95 events during the 2015-2024 late historical period. Shading shows resampling and iteration number used in the manuscript main text.

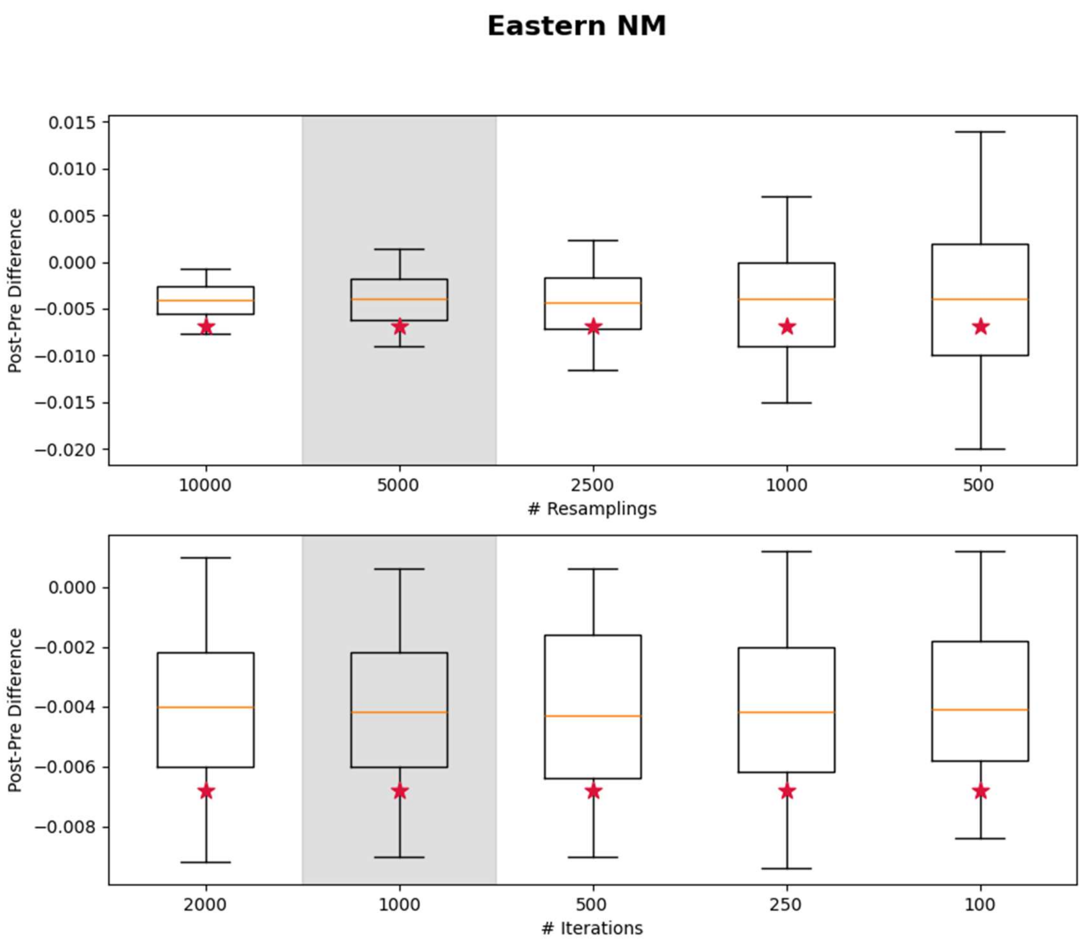

Figure S13: Bootstrapping sensitivity test for grid cell in eastern New Mexico. Box plots show the median, interquartile range, and 5th and 95th percentiles in the difference in the synthetic time series' post- versus pre-season fractional share of annual T95 events, as measured by bootstrapping tests with different numbers of resamplings and iterations. Star shows observed post- versus pre-season share of T95 events during the 2015-2024 late historical period. Shading shows resampling and iteration number used in the manuscript main text.

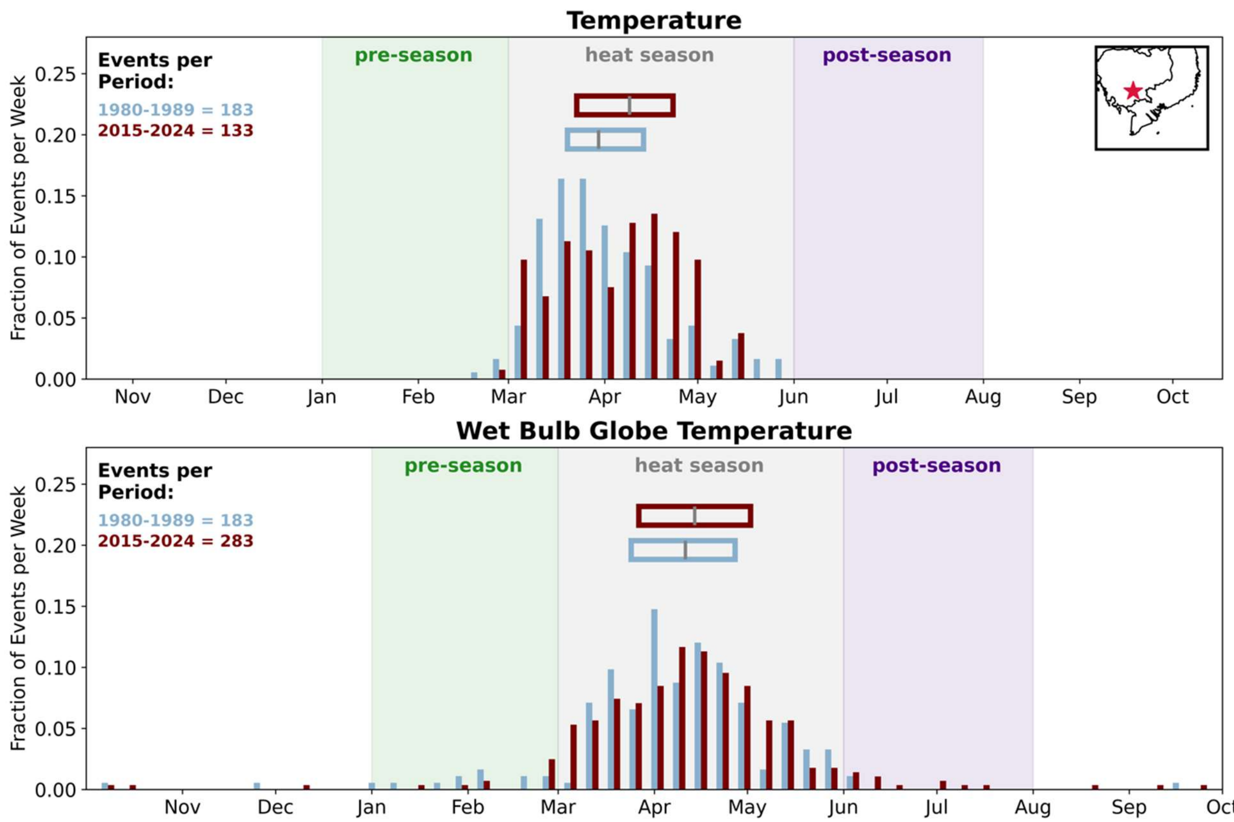

Figure S14: Analogous to Figure 1, but for a grid cell in Phnom Penh, Cambodia. City location shown by red star in upper right inset plot.

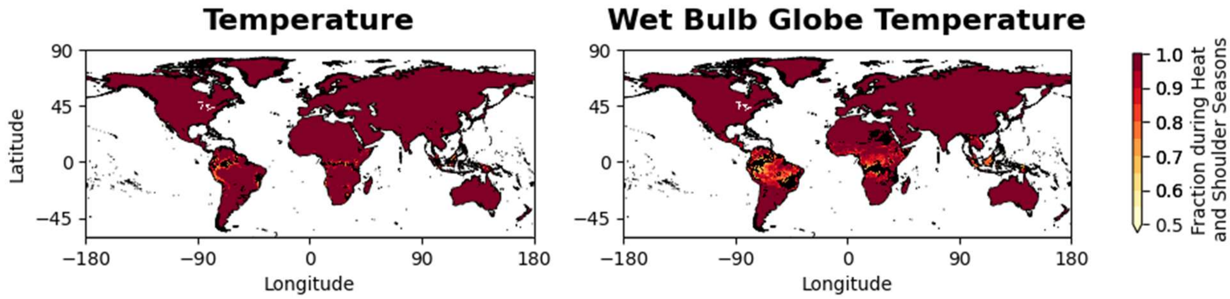

Figure S15: Fraction of 1980-1989 extremes that occur during the extreme heat and shoulder seasons, for T95 extremes (left) and WBGT95 extremes (right). Black shading indicates grid cells without a consecutive 3-month heat season.

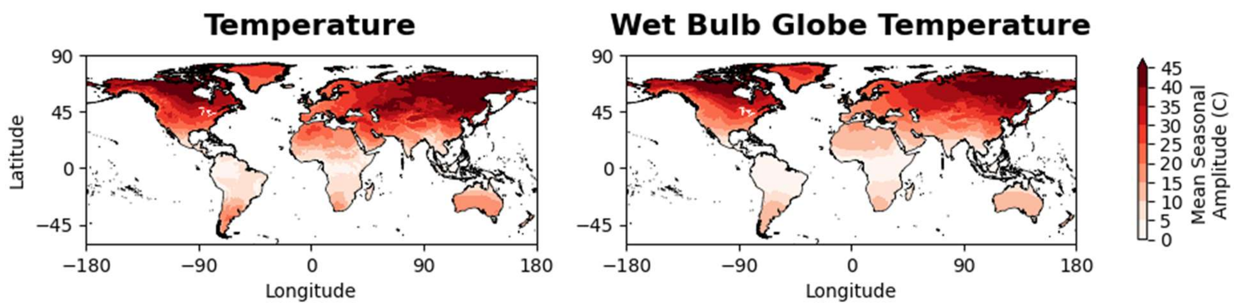

Figure S16: Mean seasonal amplitude as defined by the difference in the maximum versus minimum monthly mean temperature (left) and WBGT (right).

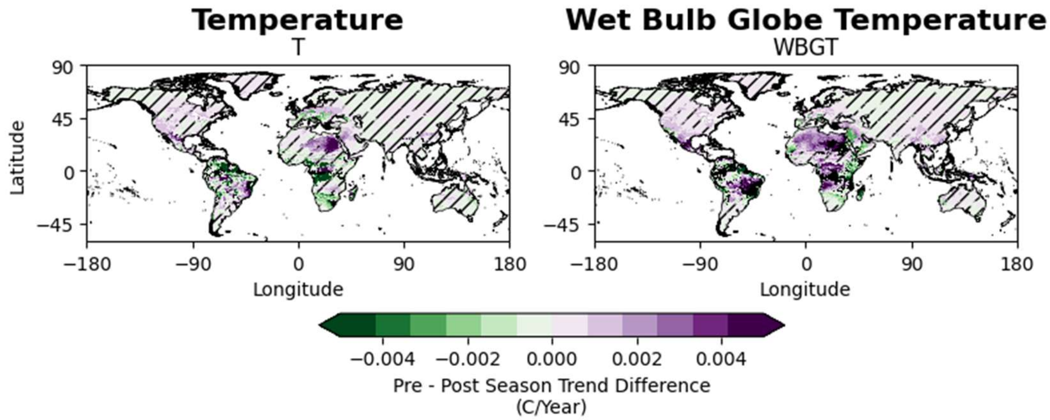

.

Figure S17: Difference in trend in annual T95 and WBGT95 counts during pre- and post-seasons defined by temperature (left) and WBGT (right) heat seasons. Linear regression calculated between 1980-2024. Hatching shows where trends in both shoulder seasons (pre- and post-seasons) are insignificant based on a p-value of 0.05.

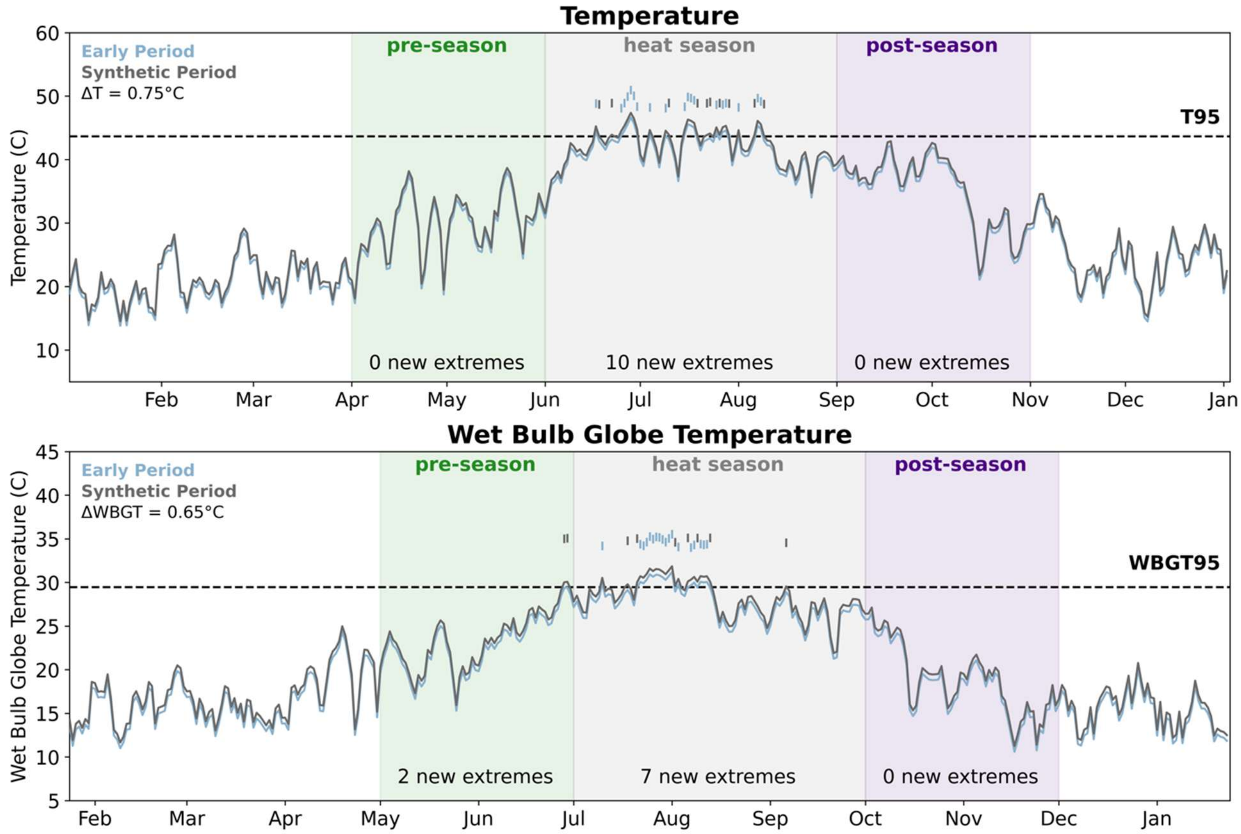

Figure S18: Visualization of existing seasonality synthetic intensification for Phoenix, AZ during the year 1980. Observed time series in 1980 shown in light blue. This observed time series is shifted up by the local temperature or WBGT delta between early and late periods, 0.75°C and 0.65°C respectively, in order to generate synthetic time series (grey). Time steps which cross the historical T95 and WBGT95 thresholds are shown by dash marks. Blue dash marks indicate extreme heat events observed in the 1980 historical record; grey dash marks indicate additional extreme heat events in the synthetic distribution associated with the shifting up of the time series. This total number of additional extremes in the synthetic period is annotated at the bottom of the plot for each season.

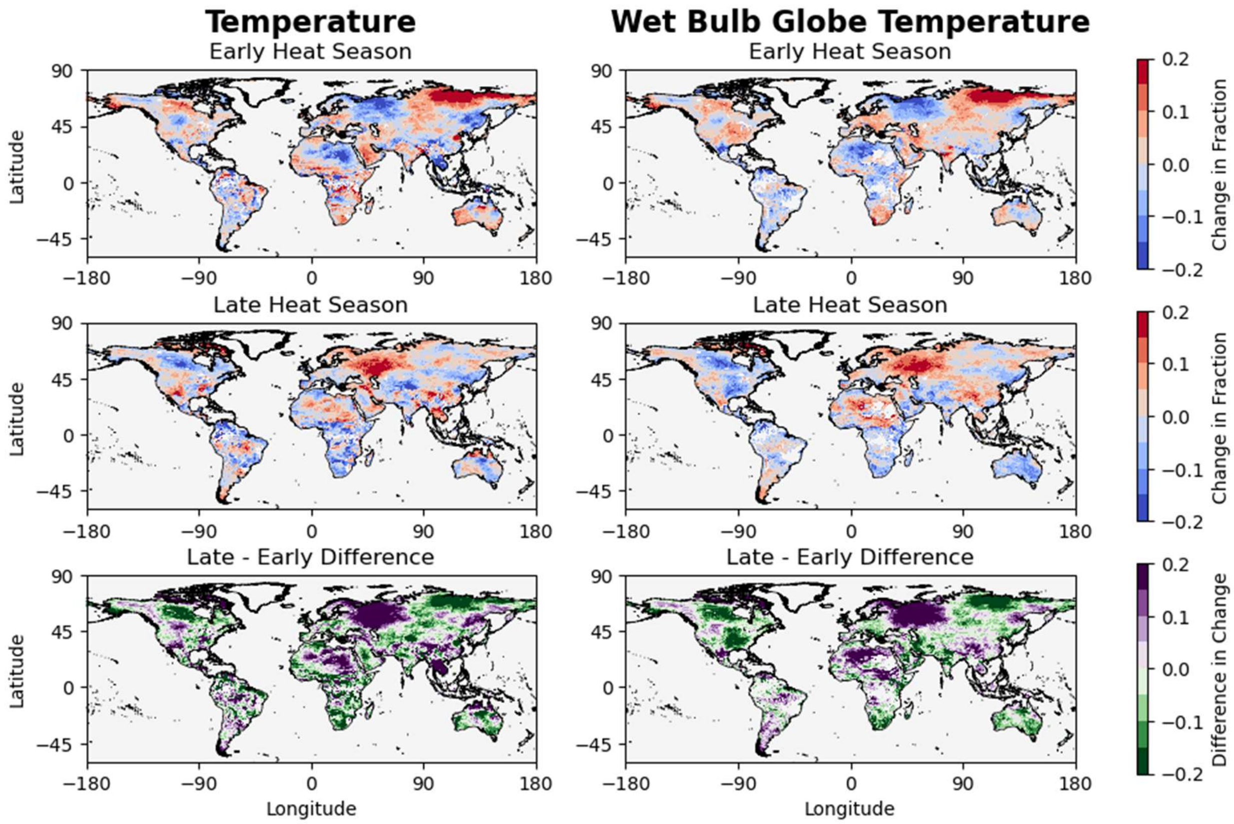

Figure S19: Asymmetry in extreme heat occurring in the first and last months of the heat season.

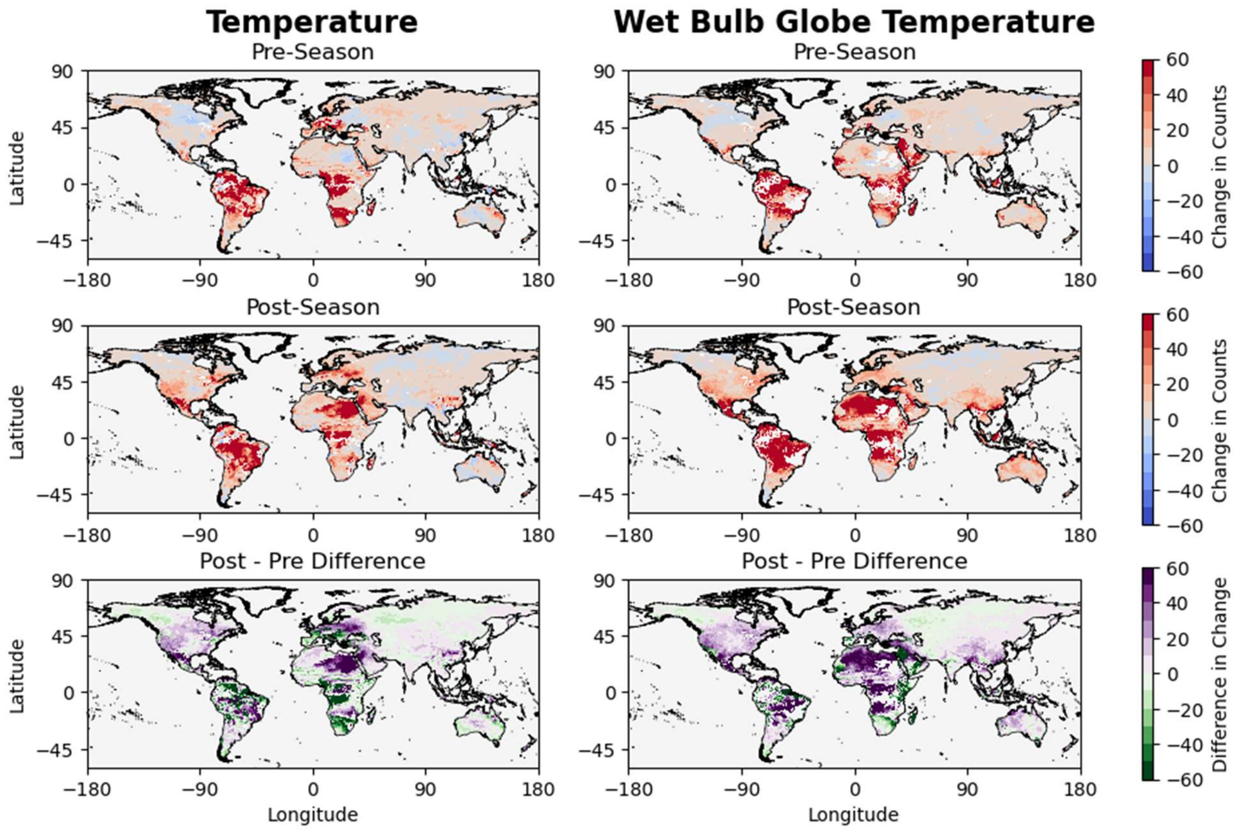

Figure S20: Analogous to Figure 4, but for event counts instead of fraction of events per year.